COMMUNICATIONS PHYSICS

ARTICLE

https://doi.org/10.1038/s42005-020-0342-2 OPEN

Phase diagram of the two-dimensional Hubbard-Holstein model

Natanael C. Costa[1,2]✉, Kazuhiro Seki[3], Seiji Yunoki[3,4,5] & Sandro Sorella[1]

The electron–electron and electron–phonon interactions play an important role in correlated materials, being key features for spin, charge and pair correlations. Thus, here we investigate their effects in strongly correlated systems by performing unbiased quantum Monte Carlo simulations in the square lattice Hubbard-Holstein model at half-filling. We study the competition and interplay between antiferromagnetism (AFM) and charge-density wave (CDW), establishing its very rich phase diagram. In the region between AFM and CDW phases, we have found an enhancement of superconducting pairing correlations, favouring (nonlocal) *s*-wave pairs. Our study sheds light over past inconsistencies in the literature, in particular the emergence of CDW in the pure Holstein model case.

[1] International School for Advanced Studies (SISSA), Via Bonomea 265, Trieste 34136, Italy. [2] Instituto de Física, Universidade Federal do Rio de Janeiro Cx.P. 68.528, Rio de Janeiro RJ 21941-972, Brazil. [3] Computational Quantum Matter Research Team, RIKEN, Center for Emergent Matter Science (CEMS), Saitama 351-0198, Japan. [4] Computational Materials Science Research Team, RIKEN Center for Computational Science (R-CCS), Kobe, Hyogo 650-0047, Japan. [5] Computational Condensed Matter Physics Laboratory, RIKEN Cluster for Pioneering Research (CPR), Wako, Saitama 351-0198, Japan. ✉email: natanael@if.ufrj.br

The electron–phonon (*e-ph*) interaction is a central issue in condensed matter, in particular when discussing properties of conventional superconductivity (SC) and charge ordering[1]. While Bardeen, Cooper and Schrieffer used this interaction in their seminal work to explain pairing[2], Peierls took it into account to provide a mechanism, based on Fermi surface nesting (FSN), that leads to charge-density wave (CDW)[3]. Recently, the debate about the role of the *e-ph* coupling has been intensified due to the occurrence of unconventional (non Peierls-like) CDW phases, and their competition with SC, in some classes of materials, such as transition-metal dichalcogenides[4–7]. Even for cuprates, materials known by their strong electron–electron (*e-e*) interactions, recent findings provided evidence for the occurrence of CDW in the doped region, with competing effects with SC[7–10], e.g., on doped $La_{2-x}Ba_xCuO_4$ and $YBa_2Cu_3O_{6+x}$[11–14]. These results have suggested that the phase diagram of high-T_c superconductors[15] is far more complex than previously supposed, and have raised issues about the relevance of the *e-ph* coupling for correlated materials, rather than just *e-e* interactions.

From a theoretical point of view, a simplified Hamiltonian that captures the interplay between antiferromagnetism (AFM), CDW, and SC is the single-band Hubbard-Holstein model (HHM)[16]. It exhibits Coulomb repulsion between electrons, leading to spin fluctuations; and also electron-ion interactions, which enhance charge/pairing correlations. The emergence of long-range order depends on the competition between these tendencies. This model was vastly studied in one-dimensional systems, with well-known phase diagrams presenting spin-density wave, bond-order-wave, CDW, and also metallic or phase separation behavior[17–24]. A remarkable feature in 1D systems is the occurrence of a quantum phase transition from a metallic Luther-Emery liquid phase[25] to a CDW insulator at a finite critical *e-ph* coupling, in the limit case of the pure Holstein model ($U = 0$), despite of the FSN[26,27]. By contrast, the properties of the HHM in two-dimensional systems are not entirely clear, even for simple geometries, such as the square lattice. For instance, the existence of such a metal-CDW quantum critical point (QCP) is matter of controversies for the pure Holstein model in 2D lattices[28–33]. The scenario is much less clear in presence of a repulsive Hubbard term ($U \neq 0$), in spite of the large effort to characterize the model[16,31–44], since no unbiased results are available for quantum AFM/CDW transitions, to the best of our knowledge.

In view of these open issues, and as a step towards a better understanding of the role of *e-ph* interactions in strongly interacting systems, we investigate in this article the competition between AFM and CDW in the square lattice HHM at half-filling, as well as its pairing response, using unbiased quantum Monte Carlo (QMC) simulations. We determine precise critical points for the HHM at intermediate interaction strengths, presenting benchmarks for lattices with linear size up to $L = 48$ (i.e., 2304 sites) in some cases. Our main results are summarized in the ground state phase diagram displayed in Fig. 1. Here we highlight [i] the absence of a finite critical *e-ph* coupling for the pure Holstein model, i.e., the CDW phase sets in for any $\lambda > 0$ (and $U = 0$); [ii] the existence of a finite AFM critical point on the line $U = \lambda$, which is strongly dependent on the phonon frequency; and [iii] an enhancement of nonlocal *s*-wave pairing in the region between the AFM and CDW phases. These results are also compared with other methodological approaches, such as variational QMC.

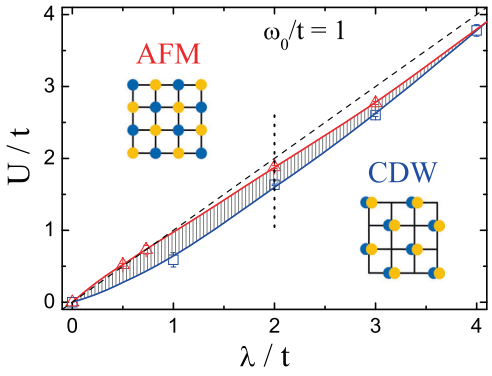

Fig. 1 Phase diagram. Ground state phase diagram of the Hubbard-Holstein model at the half-filling of the square lattice, and adiabaticity ratio $\omega_0/t = 1$. The hatched region exhibits a correlated metallic (or superconducting) behavior. The dashed line defines $U = \lambda$, while the solid lines are guide to the eyes. The red and blue lines correspond to the antiferromagnetic (AFM) and charge-density wave (CDW) transitions, respectively. When not shown, error bars are smaller than symbol size.

Results

The model. The Hubbard-Holstein Hamiltonian reads

$$\mathcal{H} = -t\sum_{\langle \mathbf{i},\mathbf{j}\rangle,\sigma}\left(d^{\dagger}_{\mathbf{i}\sigma}d^{\dagger}_{\mathbf{j}\sigma} + \text{h.c.}\right) - \mu\sum_{\mathbf{i},\sigma} n^{\dagger}_{\mathbf{i},\sigma} + U\sum_{\mathbf{i}} n_{\mathbf{i}\uparrow}n_{\mathbf{i}\downarrow} + \sum_{\mathbf{i}}\left(\frac{\hat{P}^2_{\mathbf{i}}}{2M} + \frac{M\omega_0^2}{2}\hat{X}^2_{\mathbf{i}}\right) - g\sum_{\mathbf{i},\sigma} n_{\mathbf{i}\sigma}\hat{X}_{\mathbf{i}}, \quad (1)$$

where $d^{\dagger}_{\mathbf{i}\sigma}$ ($d_{\mathbf{i}\sigma}$) is a creation (annihilation) operator of electrons with spin $\sigma(=\uparrow,\downarrow)$ at a given site $\mathbf{i}$ on a two-dimensional square lattice under periodic boundary conditions, with $\langle \mathbf{i}, \mathbf{j}\rangle$ denoting nearest-neighbors, and $n_{\mathbf{i}\sigma} \equiv d^{\dagger}_{\mathbf{i}\sigma}d_{\mathbf{i}\sigma}$ being number operators. The first two terms on the right hand side of Eq. (1) correspond to the kinetic energy of electrons, and their chemical potential (μ) term, respectively, while the on-site Coulomb repulsion between electrons is included by the third term. The ions' phonon modes are described in the fourth term, in which $\hat{P}_{\mathbf{i}}$ and $\hat{X}_{\mathbf{i}}$ are momentum and position operators, respectively, of local quantum harmonic oscillators with frequency ω_0. The last term corresponds to local electron-ion interactions, with strength g. Hereafter, we define the mass of the ions (M) and the lattice constant as unity.

It is also worth to introduce additional parameters, due to the effects of the phonon fields to the electronic interactions. From a second order perturbation theory on the *e-ph* term[16], one obtains an effective dynamic *e-e* interaction, $U_{\text{eff}}(\omega) = U - \frac{g^2/\omega_0^2}{1-(\omega/\omega_0)^2}$, with $g^2/\omega_0^2 \equiv \lambda$ being the energy scale for polaron formation. The appearance of such a retarded attractive interaction, depending on the phonon frequency, leads us to define ω_0/t as the adiabaticity ratio, and λ/t as the strength of the *e-ph* interaction. To facilitate the following discussion, we also define $U_{\text{eff}} \equiv U - \lambda$, which gives us a rough information about the local effective *e-e* interaction, and is also an important parameter to our methodological approaches. Furthermore, we set the electron density at half-filling, i.e., $\langle n_{\mathbf{i}\sigma}\rangle = 1/2$.

We investigate the properties of Eq. (1) by performing two different unbiased auxiliary-field QMC approaches: the projective ground state auxiliary-field (AFQMC)[45,46], and the finite temperature determinant quantum Monte Carlo (DQMC) methods[46–48]. Following the procedures described in Karakuzu et al.[49], we implemented a sign-free AFQMC approach to the half-filling of the HHM, allowing us to analyze large lattice sizes, but, conversely, being restricted to the $U_{\text{eff}} \geq 0$ region. The properties of the $U_{\text{eff}} < 0$ region, forbidden to our AFQMC method, are investigated by DQMC simulations. We recall that the DQMC method may exhibit sign problem for the HHM, depending on the strength of parameters. However, as shown in the Supplementary Figure 4, the values for the average sign with $U < \lambda$ are still suitable for performing accurate simulations for the CDW phase, in particular for intermediate interaction strengths,

allowing us to obtain the physical quantities of interest, in some cases up to $L = 14$ and $\beta = 1/T = 28$. In fact, the DQMC average sign is strongly suppressed just around $U \approx \lambda$, where our sign-free AFQMC approach works. Thus, our AFQMC and DQMC simulations are used complementarily.

The charge and magnetic responses are quantified by their respective structure factors, i.e., $S_{\rm cdw}(\mathbf{q}) = \frac{1}{N}\sum_{\mathbf{i},\mathbf{j}} e^{-i\mathbf{q}\cdot(\mathbf{i}-\mathbf{j})}\langle n_{\mathbf{i}} n_{\mathbf{j}}\rangle$, and $S_{\rm afm}(\mathbf{q}) = \frac{1}{N}\sum_{\mathbf{i},\mathbf{j}} e^{-i\mathbf{q}\cdot(\mathbf{i}-\mathbf{j})}\langle S^z_{\mathbf{i}} S^z_{\mathbf{j}}\rangle$, with $n_{\mathbf{i}} = n_{\mathbf{i}\uparrow} + n_{\mathbf{i}\downarrow}$, $S^z_{\mathbf{i}} = n_{\mathbf{i}\uparrow} - n_{\mathbf{i}\downarrow}$, and $N = L \times L$ being the number of sites. This allows us to probe their critical behavior by means of the correlation ratio

$$R_\nu(L) = 1 - \frac{S_\nu(\mathbf{q}+\delta\mathbf{q})}{S_\nu(\mathbf{q})}, \qquad (2)$$

with $|\delta\mathbf{q}| = 2\pi/L$, $\mathbf{q} = (\pi, \pi)$, and $\nu \equiv$ cdw or afm. According to well established finite size scaling analysis, the critical region is determined by the crossing points of $R_\nu(L)$ for different lattice sizes[50–53]. Finally, the pairing properties are investigated by the finite temperature superconducting pair susceptibility $\chi^\alpha_{\rm sc}(\beta) = \frac{1}{N}\int_0^\beta d\tau\, \langle \Delta_\alpha(\tau)\Delta^\dagger_\alpha(0)\rangle$, with $\Delta_\alpha(\tau) = \frac{1}{2}\sum_{\mathbf{i},\mathbf{a}} f_\alpha(\mathbf{a}) c^\dagger_{\mathbf{i}\downarrow}(\tau) c^\dagger_{\mathbf{i}+\mathbf{a}\uparrow}(\tau)$, $c_{\mathbf{i}\sigma}(\tau) = e^{\tau\mathcal{H}} c_{\mathbf{i}\sigma} e^{-\tau\mathcal{H}}$ and $f_\alpha(\mathbf{a})$ being the pairing form factor for a given symmetry. Here, we consider on-site, nearest-neighbors (NN), and next-nearest-neighbors (NNN) spin-singlet pairing operators for the s-wave symmetry, which are denoted by $\alpha \equiv s$, s^*, and s^{**} (or s_{xy}, as also called in literature), respectively; and also consider the $d_{x^2-y^2}$-wave symmetry, $\alpha \equiv d$ (see, e.g., White et al.[54]).

The Holstein model ($U = 0$). We first discuss the limit case of $U = 0$ in Eq. (1), i.e., the pure Holstein model. While the Peierls' argument[55] suggests an insulating charge ordered ground state for any $\lambda > 0$, one-dimensional systems exhibit a metal-CDW transition for a finite critical λ_c, despite the perfect FSN. In two dimensions, the occurrence of a finite critical λ_c in the square lattice is controversial: while variational QMC approaches provide evidence for $\lambda_c/t \approx 0.8$[32,33], unbiased QMC results suggest the nonexistence of a finite critical point[30,31]. Here, we address this controversy by analyzing the critical behavior given by the CDW correlation ratio, Eq. (2), by means of DQMC simulations One should notice that, for $U = 0$, the DQMC method does not suffer with the sign problem, allowing us to investigate larger lattice sizes and lower temperatures.

The quantum critical region is probed by the behavior of the correlation ratio as a function of the *e-ph* coupling, and projecting on the ground state by using $\beta \sim L$, for different system sizes. Fig. 2 displays the $R_{\rm cdw}(L)$ as a function of λ/t for several lattice sizes, fixing $U = 0$ and $\beta = 2L$. Here, we start discussing the possible existence of a CDW quantum phase transition at $\lambda_c/t \approx 0.8$, as suggested by variational methods. By fixing $\lambda/t = 0.8$, we notice that the correlation ratio increases monotonically as a function of the lattice size, clearly supporting long-range CDW order in the thermodynamic limit, at this interaction strength and above, in line with Hohenadler et al.[30]. In fact, one may estimate the QCP by the value of λ/t determined by a crossing of $R_{\rm cdw}(L)$ for different system sizes. Here we define $\lambda_c(L, L-\Delta L)$ as the size-dependent critical coupling obtained by the crossing between $R_{\rm cdw}(L)$ and $R_{\rm cdw}(L-\Delta L)$. As presented in the inset of Fig. 2, the values of $\lambda_c(L, L-\Delta L)$ are smaller than the one suggested by the variational methods, and they also are reduced when L increases. Given this, whether a metal-insulator transition exists, it should occur at smaller coupling strengths.

A thorough determination of the existence of a critical point is given by a finite size scaling analysis of $\lambda_c(L, L-\Delta L)$. Following the procedure adopted in Weber et al.[31], which hereafter is used to determine the CDW transitions, we perform a power law fit

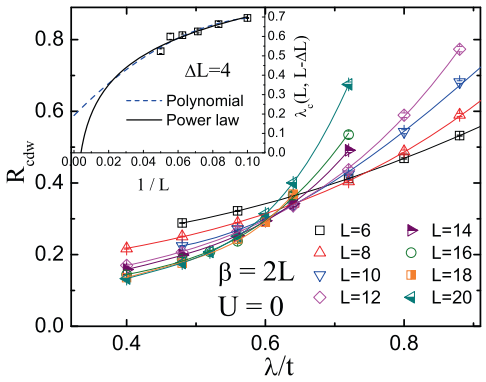

Fig. 2 Charge correlation ratio for the Holstein model. Determinant quantum Monte Carlo results for the charge-density wave correlation ratio, Eq. (2), as function of λ/t, for different lattice sizes, and by fixing $\beta = 2L$, $\omega_0/t = 1$, and $U = 0$. The solid lines are just guide to the eyes. Inset: $\lambda_c(L, L-\Delta L)$ as a function of $1/L$; the solid (dashed) curve corresponds to its power law (polynomial) scaling. When not shown, error bars are smaller than symbol size.

$[f(L) = a + bL^c]$ of the crossing points, as displayed in the inset of Fig. 2. Within this scaling analysis, the critical coupling (at $L \to \infty$) λ_c for $U = 0$ is consistent with a vanishing or very small value, even when we adopt the less accurate (2nd order) polynomial fit. Similar analysis for a different ground state projection, i.e. $\beta \sim L^2$, also agrees with a vanishing λ_c for $U = 0$; see also the Supplementary Notes 1. That is, these results provide evidence that a finite critical *e-ph* coupling is not plausible for the square lattice Holstein model. The difference between the square lattice and one-dimensional systems may stem on the larger electronic susceptibility of the former, which diverges with the square logarithm of temperature.

The Hubbard-Holstein model. We now turn to discuss the behavior of the HHM for $U \neq 0$, investigating initially the particular case of $U = \lambda$, by means of AFQMC simulations. We recall that the HHM in the $\omega_0 \to \infty$ limit is equivalent to the Hubbard model with an onsite interaction $U_{\rm eff}$. Then, it should exhibit a metallic behavior along the line $U = \lambda$ in this case. However, the existence of finite phonon frequencies leads to a retarded interaction, therefore to a more complex ground state. Indeed, our AFQMC results for $\omega_0/t \leq 1$ exhibit an enhancement of the spin-spin correlations as a function of U/t, on the line $U = \lambda$, as showed in the Supplementary Fig. 1. Conversely, the charge-charge response remains weak for any interaction strength, suggesting that an AFM order sets in at ground state.

Similarly to the previous CDW analysis, the AFM long-range order is established by investigating the crossing points of the AFM correlation ratio. Fig. 3 displays the $U_c(L, \alpha L)$, i.e. the values of U/t for the crossing points of $R_{\rm afm}(L)$ and $R_{\rm afm}(\alpha L)$, for different phonon frequencies, and fixing $\beta = 2L$. Due to the large lattice sizes achieved in our AFQMC simulations, here we adopt a linear polynomial fit for the AFM transitions. As expected, the pure Hubbard model (black square symbols in Fig. 3) is AFM for any $U > 0$, i.e., $U_c = 0$. However, in presence of *e-ph* coupling (along the line $U = \lambda$), a quantum phase transition occurs, changing from a correlated metallic-like ground state to an ordered AFM one, for a given coupling strength. Dynamical mean-field theory analyses also report similar results for higher dimensionality calculations[36–38]. In our QMC simulations, for instance, one finds $U_c/t = \lambda_c/t = 0.73(6)$ by fixing $\omega_0/t = 1$; that is, the ground state is AFM for any $U = \lambda > 0.73t$. The position of this QCP strongly depends on the choice of ω_0/t, as showed in the inset of Fig. 3. A similar analysis for a different ground state

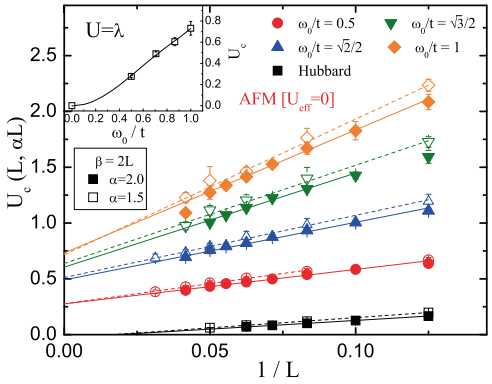

Fig. 3 Antiferromagnetic transitions for $\lambda = U$. Projective auxiliary-field quantum Monte Carlo results for the crossing points of $R_{afm}(L)$ and $R_{afm}(\alpha L)$, for different phonon frequencies, and by fixing $\beta = 2L$ and $U_{eff} = 0$. The lines are linear scalings. Inset: Critical antiferromagnetic points for $U_{eff} = 0$ as function of the phonon frequency ω_0/t. When not shown, error bars are smaller than symbol size.

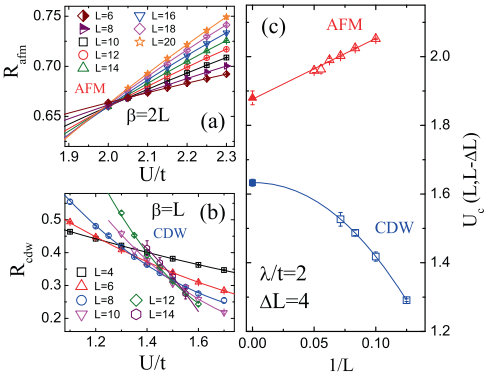

Fig. 4 Antiferromagnetic and charge-density wave transitions for $\lambda = 2t$. **a** Projective auxiliary-field quantum Monte Carlo results for the antiferromagnetic correlation ratio for $\beta = 2L$, and **b** determinant quantum Monte Carlo results for the charge-density wave correlation ratio for $\beta = L$, as function of the U/t, for different lattice sizes, and by fixing $\lambda/t = 2$ and $\omega_0/t = 1$. The solid lines are just guide to the eyes. **c** The crossing points of $R_{afm}(L)$ (red triangles), and $R_{cdw}(L)$ (blue squares), and their respective scaling curves. When not shown, error bars are smaller than symbol size.

projection ($\beta \sim L^2$) agrees with it, but suggesting slightly larger critical couplings, as presented in the Supplementary Notes . Notice that such increasing behavior of U_c as a function of ω_0 is consistent with the initial expectation of an emergent metallic behavior in the antiadiabatic limit for $U = \lambda$. The properties of this correlated metallic-like state are discussed later.

We proceed by investigating the quantum critical behavior for the general case, $U \neq \lambda$. To this end, here we analyze the AFM and CDW correlation ratios as functions of U/t, for fixed λ/t and ω_0/t, e.g., as represented by the vertical dotted line in Fig. 1. With this in mind, Fig. 4a displays AFQMC results for $R_{afm}(L)$ as function of U/t, and fixed $\lambda/t = 2$ and $\omega_0/t = 1$. The crossing points $U_c(L, L - \Delta L)$ between $R_{afm}(L)$ and $R_{afm}(L - \Delta L)$, as well as their finite size scaling, are displayed in Fig. 4c, leading to an AFM quantum phase transition at $U_c^{AFM}/t = 1.88(2)$. Similarly, the QCP for a CDW transition may be obtained by DQMC simulations of $R_{cdw}(L)$, as presented in Fig. 4b, with crossing points and finite size scaling shown in Fig. 4c, leading to $U_c^{CDW}/t = 1.63(1)$.

When the above analysis is repeated for other values of λ/t, we obtain the phase diagram presented in Fig. 1, with the QCPs being reported in the Supplementary Tables. It is worth mentioning that, for the range of parameters analyzed, we obtain continuous transitions for both AFM and CDW phases, without coexistence, and with a metallic-like (or SC) region between them. First order transitions may occur for stronger coupling, as suggested in the recent literature[32,33].

Pairing susceptibility response. Finally, it is instructive to discuss the properties of the region between AFM and CDW phases, from which it is expected the emergence of SC. Since our DQMC method exhibits a small average sign when $U \approx \lambda$, then establishing long-range SC order is challenging, and we are restricted to smaller lattice sizes and high temperatures; see, e.g., Supplementary Fig. 5. Despite this, one is able to investigate the SC properties by analyzing the tendency of the pairing susceptibility as a function of the temperature. For instance, Fig. 5a displays the behavior of $\chi_{\alpha(sc)}$ for fixed $\lambda/t = 2$, and $U/t = 1.7$. Here, we notice an enhancement in the pairing correlations at low temperature, with the dominant symmetry being the d-wave[41,44].

However, a better estimation for pairing is given by extracting the particle-particle contribution of $\chi_{\alpha(sc)}$. Thus, here we define the effective pair (vertex) susceptibility[54] as $\chi^{eff}_{\alpha(sc)} = \chi_{\alpha(sc)} - \bar{\chi}_{\alpha(sc)}$, with $\bar{\chi}_{\alpha(sc)}$ being the noninteracting susceptibility. A positive

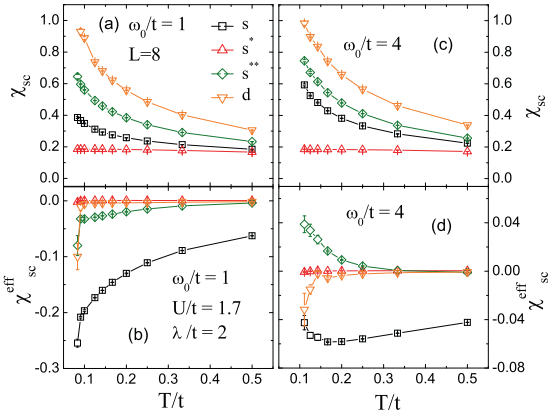

Fig. 5 Finite temperature pair susceptibility. Determinant quantum Monte Carlo results for the pair susceptibility as function of temperature T, for fixed $\lambda/t = 2$, $U/t = 1.7$, $L = 8$, and **a** $\omega_0/t = 1$ and **c** $\omega_0/t = 4$, and their respective effective susceptibilities for **b** $\omega_0/t = 1$ and **d** $\omega_0/t = 4$. When not shown, error bars are smaller than symbol size.

(negative) response of $\chi^{eff}_{\alpha(sc)}$ corresponds to an enhancement (weakening) of an attractive pair channel for the αth symmetry. Fig. 5b exhibits $\chi^{eff}_{\alpha(sc)}$ for the data of panel (a), showing negative tendency towards all of the examined channels. In particular, the on-site s-wave has the largest negative response, which shows the harmfulness of the Hubbard-like term for local pairs formation. However, since $T_{sc} \sim \omega_0$ from the BCS theory[2], further insights about the nature of this region may be given by increasing ω_0, while keeping U_{eff} fixed, as displayed in Fig. 5c, d, for $\omega_0/t = 4$, $\lambda/t = 2$, and $U/t = 1.7$. For these parameters, despite the increasing dominant behavior of $\chi_{\alpha(sc)}$ for the d-wave, only the NNN s-wave exhibits a positive effective susceptibility. Thus, these combined features suggest that, whether SC emerges at ground state, it likely is (nonlocal) s-wave.

Indeed, since this metallic-like region seems to be in the negative U_{eff} side of the phase diagram in Fig. 1, the s-wave symmetry is naively expected. Interestingly, such an enhancement of nonlocal s-wave response suggests that short-range charge/spin correlations may suppress the formation of local (s-wave) and NN (s^*-wave) Cooper pairs, making the NNN ones (s^{**}-wave) the

main channel for pairing. It is also important to notice that, as a consequence of the Kohn-Luttinger weak coupling argument[56], instabilities in the particle-particle channel are expected in this intermediate region without AFM and CDW orders, which could lead to pairing[57–59]. However, these instabilities are believed to occur at very low temperatures, usually not accessible for the current QMC methodologies. Finally, we warn that a more precise determination of the nature of this region may also require the analysis of dynamical quantities, or long-range effective electronic interactions[43,60].

Discussion

We have presented results for the HHM in the square lattice, using unbiased AFQMC and DQMC methods complementarily, which provide a broader picture about the physical responses of this model. In particular, we have shown that, different from one-dimensional systems, the emergence of the CDW phase in the square lattice occurs for any $\lambda > 0$, for $U = 0$. However, these CDW correlations are strongly affected by a Coulomb interaction ($U \neq 0$), with the occurrence of AFM even at $U_{\mathrm{eff}} < 0$. We also observed the existence of a correlated metallic-like region between CDW and AFM phases, with an enhancement of nonlocal *s*-wave pairing, rather than *d*-wave. Despite the difficulty to establish long-range order for SC, one may expect that *s*-wave SC sets in at zero temperature.

These findings constitute a significant step towards a better understanding of this model, by providing precise QCPs, and shedding lights over past theoretical inconsistencies, although there still remain open questions, such as the behavior of the phase boundaries as a function of ω_0. Further investigations on a given compound may require the inclusion of its key features. In the cuprates, e.g., the electron-phonon coupling effects are due to the out-of-phase vibrations of planar oxygens along the *c*-axis, the B_{1g} phonon mode, which is momentum dependent (i.e., it is not Holstein-like), and favors *d*-wave symmetry[61,62]. However, doing this would also demand an increasing degree of complexity for the models considered (multi-band systems, non-Holstein phonon modes, etc)[63,64], and also a reduction in the energy scale of the phonon fields, since $\omega(\mathbf{q}) << t$ for most of the realistic materials. Apart from these specificities, the results for the HHM emphasize the fundamental role of the *e-ph* interaction in strongly correlated systems, which is important to the emergence of charge order and pairing, and may be relevant for the physics of novel correlated materials.

Methods

Quantum Monte Carlo simulations. We employed two different approaches: the DQMC and the AFQMC methods. Briefly, the DQMC (AFQMC) approach is based on the decoupling of the non-commuting terms of the Hamiltonian in the partition function (projection operator) by Trotter-Suzuki decomposition, which discretizes the imaginary-time coordinate τ in small intervals $\Delta\tau$, with the inverse of temperature T (projection time) being $\beta = M\Delta\tau$. The interacting terms are transformed in single-particle operators by means of a discrete Hubbard-Stratonovich transformation, with the cost of including bosonic auxiliary-fields $\mathcal{S}_{\mathrm{i},\tau}$, in real space and imaginary-time coordinates, coupled to fermionic degrees of freedom. Monte Carlo methodologies are used for sampling $\mathcal{S}_{\mathrm{i},\tau}$. Throughout this article, we choose $\Delta\tau t = 0.1$, with β in unit of t. Finally, in view of the large autocorrelation time, a still unsolved challenge in the DQMC method for electron-phonon systems, we restrict our analysis in the safe region of frequencies $\omega_0/t \geq 1$, when dealing with this approach (see also the Supplementary Notes 2). Detailed introduction for these methodologies can be found, e.g., in dos Santos[65], Gubernatis et al.[66], and Becca and Sorella[67].

Data availability

The datasets obtained during this work are available from the corresponding author upon reasonable request.

Code availability

Code is available upon reasonable request.

Received: 15 October 2019; Accepted: 30 March 2020;
Published online: 08 May 2020

References

1. Giustino, F. Electron-phonon interactions from first principles. *Rev. Mod. Phys.* **89**, 015003 (2017).
2. Bardeen, J., Cooper, L. N. & Schrieffer, J. R. Theory of superconductivity. *Phys. Rev.* **108**, 1175–1204 (1957).
3. Peierls, R. E. *Quantum Theory of Solids*. (Oxford University, New York, 1955).
4. CastroNeto, A. H. Charge density wave, superconductivity, and anomalous metallic behavior in 2D transition metal dichalcogenides. *Phys. Rev. Lett.* **86**, 4382–4385 (2001).
5. Rossnagel, K. On the origin of charge-density waves in select layered transition-metal dichalcogenides. *J. Phys.: Condens. Matter.* **23**, 213001 (2011).
6. Manzeli, S., Ovchinnikov, D., Pasquier, D., Yazyev, O. V. & Kis, A. 2D transition metal dichalcogenides. *Nat. Rev. Mater.* **2**, 17033 (2017).
7. Chen, C. W., Choe, J. & Morosan, E. Charge density waves in strongly correlated electron systems. *Rep. Prog. Phys.* **79**, 084505 (2016).
8. Lanzara, A., Bogdanov, P. V., Zhou, X. J., Kellar, S. A. & Feng, D. L. et al. Evidence for ubiquitous strong electron-phonon coupling in high-temperature superconductors. *Nature* **412**, 510 (2001).
9. Wise, W. D., Boyer, M. C., Chatterjee, K., Kondo, T. & Takeuchi, T. et al. Hudson, Charge-density-wave origin of cuprate checkerboard visualized by scanning tunnelling microscopy. *Nat. Phys.* **4**, 696–699 (2008).
10. DaSilvaNeto, E. H., Aynajian, P., Frano, A., Comin, R. & Schierle, E. et al. Ubiquitous interplay between charge ordering and high-temperature superconductivity in cuprates. *Science* **343**, 393–396 (2014).
11. Kim, H.-H., Souliou, S. M., Barber, M. E., Lefrançois, E. & Minola, M. et al. Uniaxial pressure control of competing orders in a high-temperature superconductor. *Science* **362**, 1040–1044 (2018).
12. Cyr-Choinière, O., LeBoeuf, D., Badoux, S., Dufour-Beauséjour, S. & Bonn, D. A. et al. Sensitivity of T_c to pressure and magnetic field in the cuprate superconductor $YBa_2Cu_3O_y$: evidence of charge-order suppression by pressure. *Phys. Rev. B* **98**, 064513 (2018).
13. Wu, T., Mayaffre, H., Krämer, S., Horvatić, M. & Berthier, C. et al. Magnetic-field-induced charge-stripe order in the high-temperature superconductor $YBa_2Cu_3O_y$. *Nature* **477**, 191–194 (2011).
14. Chang, J., Blackburn, E., Holmes, A. T., Christensen, N. B. & Larsen, J. et al. Direct observation of competition between superconductivity and charge density wave order in $YBa_2Cu_3O_{6.67}$. *Nat. Phys.* **8**, 871–876 (2012).
15. Keimer, B., Kivelson, S. A., Norman, M. R., Uchida, S. & Zaanen, J. From quantum matter to high-temperature superconductivity in copper oxides. *Nature* **518**, 179 (2015).
16. Berger, E., Valášek, P. & vonderLinden, W. Two-dimensional Hubbard-Holstein model. *Phys. Rev. B* **52**, 4806–4814 (1995).
17. Ning, W. Q., Zhao, H., Wu, C. Q. & Lin, H. Q. Phonon effects on spin-charge separation in one dimension. *Phys. Rev. Lett.* **96**, 156402 (2006).
18. Matsueda, H., Tohyama, T. & Maekawa, S. Electron-phonon coupling and spin-charge separation in one-dimensional Mott insulators. *Phys. Rev. B* **74**, 241103 (2006).
19. Hohenadler, M. & Assaad, F. F. Excitation spectra and spin gap of the half-filled Holstein-Hubbard model. *Phys. Rev. B* **87**, 075149 (2013).
20. Nocera, A., Soltanieh-ha, M., Perroni, C. A., Cataudella, V. & Feiguin, A. E. Interplay of charge, spin, and lattice degrees of freedom in the spectral properties of the one-dimensional Hubbard-Holstein model. *Phys. Rev. B.* **90**, 195134 (2014).
21. Lavanya, C. U., Sankar, I. V. & Chatterjee, A. Metallicity in a Holstein-Hubbard chain at half filling with Gaussian anharmonicity. *Sci. Rep.* **7**, 3774 (2017).
22. Li, S., Tang, Y., Maier, T. A. & Johnston, S. Phase competition in a one-dimensional three-orbital Hubbard-Holstein model. *Phys. Rev. B.* **97**, 195116 (2018).
23. Hébert, F., Xiao, B., Rousseau, V. G., Scalettar, R. T. & Batrouni, G. G. One-dimensional Hubbard-Holstein model with finite-range electron-phonon coupling. *Phys. Rev. B* **99**, 075108 (2019).
24. Xiao, B., Hébert, F., Batrouni, G. & Scalettar, R. T. Competition between phase separation and spin density wave or charge density wave order: Role of long-range interactions. *Phys. Rev. B* **99**, 205145 (2019).
25. Luther, V. J. & Emery, A. Backward scattering in the one-dimensional electron gas. *Phys. Rev. Lett.* **33**, 589–592 (1974).
26. Jeckelmann, E., Zhang, C. & White, S. R. Metal-insulator transition in the one-dimensional Holstein model at half filling. *Phys. Rev. B* **60**, 7950–7955 (1999).
27. Hohenadler, M. & Fehske, H. Density waves in strongly correlated quantum chains. *Eur. Phys. J.* **91**, 204 (2018).

28. Zhang, Y.-X., Chiu, W.-T., Costa, N. C., Batrouni, G. G. & Scalettar, R. T. Charge order in the Holstein model on a honeycomb lattice. *Phys. Rev. Lett.* **122**, 077602 (2019).
29. Chen, C., Xu, X. Y., Meng, Z. Y. & Hohenadler, M. Charge-density-wave transitions of Dirac fermions coupled to phonons. *Phys. Rev. Lett.* **122**, 077601 (2019).
30. Hohenadler, M. & Batrouni, G. G. Dominant charge density wave correlations in the holstein model on the half-filled square lattice. *Phys. Rev. B* **100**, 165114 (2019).
31. Weber, M. & Hohenadler, M. Two-dimensional Holstein-Hubbard model: critical temperature, Ising universality, and bipolaron liquid. *Phys. Rev. B* **98**, 085405 (2018).
32. Karakuzu, S., Tocchio, L. F., Sorella, S. & Becca, F. Superconductivity, charge-density waves, antiferromagnetism, and phase separation in the Hubbard-Holstein model. *Phys. Rev. B* **96**, 205145 (2017).
33. Ohgoe, T. & Imada, M. Competition among superconducting, antiferromagnetic, and charge orders with intervention by phase separation in the 2D Holstein-Hubbard model. *Phys. Rev. Lett.* **119**, 197001 (2017).
34. Khatami, E., Macridin, A. & Jarrell, M. Effect of long-range hopping on T_c in a two-dimensional Hubbard-Holstein model of the cuprates. *Phys. Rev. B* **78**, 060502 (2008).
35. Barone, P., Raimondi, R., Capone, M., Castellani, C. & Fabrizio, M. Gutzwiller scheme for electrons and phonons: The half-filled Hubbard-Holstein model. *Phys. Rev. B* **77**, 235115 (2008).
36. Bauer, J. & Hewson, A. C. Competition between antiferromagnetic and charge order in the Hubbard-Holstein model. *Phys. Rev. B* **81**, 235113 (2010).
37. Bauer, J. & Hewson, A. C. Quantum phase transition between antiferromagnetic and charge order in the Hubbard-Holstein model. *Phys. Status Solidi* **247**, 638–640 (2010).
38. Murakami, Y., Werner, P., Tsuji, N. & Aoki, H. Ordered phases in the Holstein-Hubbard model: Interplay of strong Coulomb interaction and electron-phonon coupling. *Phys. Rev. B* **88**, 125126 (2013).
39. Nowadnick, E. A., Johnston, S., Moritz, B., Scalettar, R. T. & Devereaux, T. P. Competition between antiferromagnetic and charge-density-wave order in the half-filled Hubbard-Holstein model. *Phys. Rev. Lett.* **109**, 246404 (2012).
40. Johnston, S., Nowadnick, E. A., Kung, Y. F., Moritz, B., Scalettar, R. T. & Devereaux, T. P. Determinant quantum Monte Carlo study of the two-dimensional single-band Hubbard-Holstein model. *Phys. Rev. B* **87**, 235133 (2013).
41. Nowadnick, E. A., Johnston, S., Moritz, B. & Devereaux, T. P. Renormalization of spectra by phase competition in the half-filled Hubbard-Holstein model. *Phys. Rev. B* **91**, 165127 (2015).
42. Pradhan, S. & Pai, G. V. Holstein-Hubbard model at half filling: a static auxiliary field study. *Phys. Rev. B* **92**, 165124 (2015).
43. Wang, D., Wang, W.-S. & Wangai, Q.-H. Phonon enhancement of electronic order and negative isotope effect in the Hubbard-Holstein model on a square lattice. *Phys. Rev. B* **92**, 195102 (2015).
44. Mendl, C. B., Nowadnick, E. A., Huang, E. W., Johnston, S., Moritz, B. & Devereaux, T. P. Doping dependence of ordered phases and emergent quasiparticles in the doped Hubbard-Holstein model. *Phys. Rev. B* **96**, 205141 (2017).
45. Sorella, S., Baroni, S., Car, R. & Parrinello, M. A novel technique for the simulation of interacting fermion systems. *Europhys. Lett.* **8**, 663–668 (1989).
46. Blankenbecler, R., Scalapino, D. J. & Sugar, R. L. Monte Carlo calculations of coupled boson-fermion systems. I. *Phys. Rev. D* **24**, 2278–2286 (1981).
47. Hirsch, J. E. Discrete hubbard-stratonovich transformation for fermion lattice models. *Phys. Rev. B* **28**, 4059–4061 (1983).
48. Hirsch, J. E. Two-dimensional Hubbard model: numerical simulation study. *Phys. Rev. B* **31**, 4403–4419 (1985).
49. Karakuzu, S., Seki, K. & Sorella, S. Solution of the sign problem for the half-filled Hubbard-Holstein model. *Phys. Rev. B* **98**, 201108 (2018).
50. Kaul, R. K. Spin nematics, valence-bond solids, and spin liquids in SO(n) quantum spin models on the triangular lattice. *Phys. Rev. Lett.* **115**, 157202 (2015).
51. Sato, T., Assaad, F. F. & Grover, T. Quantum Monte Carlo simulation of frustrated Kondo lattice models. *Phys. Rev. Lett.* **120**, 107201 (2018).
52. Liu, Z. H., Xu, X. Y., Qi, Y., Sun, K. & Meng, Z. Y. Itinerant quantum critical point with frustration and a non-Fermi liquid. *Phys. Rev. B* **98**, 045116 (2018).
53. Darmawan, A. S., Nomura, Y., Yamaji, Y. & Imada, M. Stripe and superconducting order competing in the Hubbard model on a square lattice studied by a combined variational Monte Carlo and tensor network method. *Phys. Rev. B* **98**, 205132 (2018).
54. White, S. R., Scalapino, D. J., Sugar, R. L., Bickers, N. E. & Scalettar, R. T. Attractive and repulsive pairing interaction vertices for the two-dimensional Hubbard model. *Phys. Rev. B* **39**, 839–842 (1989).
55. Grüner, G. *D*ensity Waves in Solids, Vol. 89 (Addison-Welsley, Reading, MA, 1994).
56. Kohn, W. & Luttinger, J. M. New mechanism for superconductivity. *Phys. Rev. Lett.* **15**, 524–526 (1965).
57. Hlubina, R., Sorella, S. & Guinea, F. Ferromagnetism in the two dimensional $t-t'$ Hubbard model at the van Hove density. *Phys. Rev. Lett.* **78**, 1343–1346 (1997).
58. Hlubina, R. Phase diagram of the weak-coupling two-dimensional $t-t'$ Hubbard model at low and intermediate electron density. *Phys. Rev. B* **59**, 9600–9605 (1999).
59. Deng, Y., Kozik, E., Prokof'ev, N. V. & Svistunov, B. V. Emergent BCS regime of the two-dimensional fermionic Hubbard model: Ground-state phase diagram. *EPL Europhys. Lett.* **110**, 57001 (2015).
60. Wang, Y., Esterlis, I., Shi, T., Cirac, J. I. & Demler, E. Zero-temperature phases of the 2D Hubbard-Holstein model: A non-Gaussian exact diagonalization study. Preprint at https://arxiv.org/abs/1910.01792 (2019).
61. Devereaux, T. P., Cuk, T., Shen, Z.-X. & Nagaosa, N. Anisotropic electron-phonon interaction in the cuprates. *Phys. Rev. Lett.* **93**, 117004 (2004).
62. Cuk, T., Baumberger, F., Lu, D. H., Ingle, N. & Zhou, X. J. et al. Coupling of the B_{1g} phonon to the antinodal electronic states of $Bi_2Sr_2Ca_{0.92}Y_{0.08}Cu_2O_{8+\delta}$. *Phys. Rev. Lett.* **93**, 117003 (2004).
63. Li, S., Khatami, E. & Johnston, S. Competing phases and orbital-selective behaviors in the two-orbital Hubbard-Holstein model. *Phys. Rev. B* **95**, 121112 (2017).
64. Li, S. & Johnston, S. Quantum Monte Carlo study of lattice polarons in the two-dimensional multi-orbital Su-Schrieffer-Heeger model. Preprint at https://arxiv.org/abs/1901.07612 (2019).
65. dosSantos, R. R. Introduction to quantum Monte Carlo simulations for fermionic systems. *Braz. J. Phys.* **33**, 36–54 (2003).
66. Gubernatis, J., Kawashima, N. & Werner, P. *Quantum Monte Carlo Methods: Algorithms for Lattice Models*. (Cambridge University Press, Cambridge, England, 2016).
67. Becca, F. & Sorella, S. *Quantum Monte Carlo Approaches for Correlated Systems*. (Cambridge University Press, Cambridge, England, 2017).

Acknowledgements

We are grateful to Yuichi Otsuka for valuable discussions. Computational resources were provided by HOKUSAI supercomputer at RIKEN (Project ID: G19010), and CINECA supercomputer (PRACE-2019204934). S.S. and N.C.C. acknowledge PRACE for awarding them access to Marconi at CINECA, Italy. N.C.C. also acknowledge the financial support from the Brazilian Agencies CAPES and CNPq. This work was partially supported by Grant-in-Aid for Research Activity start-up (No. JP19K23433) from MEXT, Japan.

Author contributions

S.Y. and S.S. conceived the project. N.C.C implemented the determinant quantum Monte Carlo code, and K.S. the projective auxiliary-field quantum Monte Carlo code. The simulations were carried out by N.C.C. and K.S. under the guidance of S.Y. and S.S. All authors participated to the discussions during the writing of the article.

Competing Interests

The authors declare no competing financial interests.

Additional information

Supplementary information is available for this paper at https://doi.org/10.1038/s42005-020-0342-2.

Correspondence and requests for materials should be addressed to N.C.C.

Reprints and permission information is available at http://www.nature.com/reprints

Publisher's note Springer Nature remains neutral with regard to jurisdictional claims in published maps and institutional affiliations.